exo-**25**, 114906-86-4; *endo*-**25**, 114976-80-6; **28**, 114942-88-0; **30x**, 114942-90-4; **30n**, 115014-28-3; **31xa**, 114906-84-2; **31xs**, 114976-78-2; **31na**, 114976-79-3; **31ns**, 115014-29-4; **32xa**, 114942-91-5; **32xs**, 115014-30-7; **32na**, 115014-34-1; **32ns**, 115014-38-5; **33xa**, 114942-92-6; **33xa** (acid), 114942-95-9; **33xs**, 115014-31-8; **33xs** (acid), 115014-42-1; **33na**, 115014-35-2; **33na** (acid), 115014-43-2; **33ns**, 115014-39-6; **33ns** (acid), 115014-44-3; **34xa**, 114942-93-7; **34xs**, 115014-32-9; **34na**, 115014-36-3; **34ns**, 115014-40-9; **35xa**, 114942-94-8; **35xs**, 115014-33-0; **35na**, 115014-37-4; **35ns**, 115014-41-0; 2,4,6-$(MeO)_3C_6H_2Et$, 67827-55-8; 2,4,6-$(MeO)_3C_6H_2CH{=}CH_2$, 40243-91-2; robustadial A, 88130-99-8; robustadial B, 88197-30-2.

Robustadials. 4. Molecular Mechanics and Nuclear Magnetic Resonance Studies of Conformational and Configurational Equilibria: 3,4-Dihydrospiro[2*H*-1-benzopyran-2,2′-bicyclo[2.2.1]heptanes][1]

Michael R. Jirousek, Samuel M. Mazza, and Robert G. Salomon*

Department of Chemistry, Case Western Reserve University, Cleveland, Ohio 44106-2699

Received November 29, 1987

Conformational information obtained by molecular mechanics calculations aided in the interpretation of ^1H NMR experiments employed in the structural characterization of all four possible diastereomeric 3,4-dihydro-4-(2-methylpropyl)spiro[2*H*-1-benzopyran-2,2′-bicyclo[2.2.1]heptanes] **1**. The facile interconversion of energetically similar conformers of endo–trans (NT) and exo–trans (XT) diastereomers of **1** predicted by molecular mechanics calculations was verified by the observation of temperature-dependent changes of chemical shifts in the ^1H NMR spectra of these diastereomers. Molecular mechanics calculations also provided a good prediction of the configurational equilibrium which could be established under basic catalysis between two epimeric 3,4-dihydrospiro[2*H*-1-benzopyran-4-one-2,2′-bicyclo[2.2.1]heptanes] *endo*-**2** and *exo*-**2**.

Modern FT-NMR techniques have been employed to characterize remarkably complex organic structures without the need for X-ray crystal structural analysis. These methods are especially important for noncrystalline substances. Quaternary carbons complicate NMR analysis, especially of stereostructure, by precluding vicinal coupling of hydrogen atoms between regions of the molecule that are separated by the quaternary atom. Nuclear Overhauser effects (NOE) can bridge the gap. Nevertheless, the frequency of erroneous structural conclusions[2] makes it evident that additional approaches are needed for the accurate determination of molecular structures without the use of X-ray analysis. While NMR experiments are useful for unravelling questions of molecular conformation in solution, we considered the possibility that the reverse might also be true. That is, conformational information, available by molecular mechanics calculations, might be useful for interpreting NMR experiments to answer questions about molecular architecture. We now report a molecular mechanics conformational analysis and ^1H NMR studies that led to complete stereostructural characterization of all four possible diastereomeric 3,4-dihydro-4-(2-methylpropyl)spiro[2*H*-1-benzopyran-2,2′-bicyclo[2.2.1]heptanes] **1**, intermediates prepared in conjunction with our studies on the structures of robustadials.[1,3]

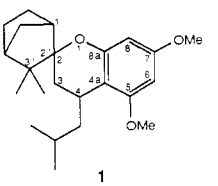

1

Results and Discussion

Conformation and Conformational Equilibria of Four Diastereomers. The possible conformational flexibility of the pyran ring in the four diastereomers of **1** complicates quantitative analysis of their ^1H NMR spectra. Thus, interactions between remote portions of such molecules depend on precise spatial relationships. We modeled the conformations of the diastereomers by using molecular mechanics calculations to aid in interpretation of NOE experiments and in analysis of temperature-dependent effects on the chemical shifts of the camphane methyl groups. The MMP2 program[4] was used to model the conformational dynamics of the diastereomers. The stabilities of conformers can be compared by calculation of their steric energies, the direct sum of the force-field increments.[4] These steric energies represent the thermally averaged energies relative to the same molecule but with all bond lengths, bond angles, and torsional angles set to their strainless values and the atoms having van der Waals and electrostatic interactions corresponding to infinite

(1) For previous paper in this series, see: Mazza, S. M.; Lal, K.; Salomon, R. G. *J. Org. Chem.*, second of three papers in this issue.

(2) For examples, see the following. (a) Robustadials. Xu, R.; Snyder, J. K.; Nakanishi, K. *J. Am. Chem. Soc.* **1984**, *106*, 734. Refuted in: Lal, K.; Zarate, E. A.; Youngs, W. J.; Salomon, R. G. *J. Am. Chem. Soc.* **1986**, *108*, 1311. (b) Azadirachtin. Zanno, P. R.; Miura, I.; Nakanishi, K. *J. Am. Chem. Soc.* **1975**, *97*, 1975. Revised by: Kraus, W.; Bokel, M.; Klenk, A.; Pöhnl, H. *Tetrahedron Lett.* **1985**, *26*, 6435 and Broughton, H. B.; Ley, S. V.; Slawin, A. M. Z.; Williams, D. J.; Morgan, E. D. *J. Chem. Soc., Chem. Commun.* **1986**, 46. (c) Stoechospermol. Solimabi, L. F.; Kamat, S. Y.; Paknikar, S. K. *Tetrahedron Lett.* **1980**, *21*, 2249. Revised by: Gerwick, W. H.; Fenical, W.; Sultanbawa, M. U. S. *J. Org. Chem.* **1981**, *46*, 2233. (d) Xylomollin. Kubo, I.; Miura, I.; Nakanishi, K. *J. Am. Chem. Soc.* **1976**, *98*, 6704. Revised by: Nakane, M.; Hutchinson, C. R.; VanEngen, D.; Clardy, J. *J. Am. Chem. Soc.* **1978**, *100*, 7079. (e) Specionin. Conway, C.; Nakanishi, K. *J. Chem. Soc., Chem. Commun.* **1983**, 605. Revised by Van der Eycken, E.; Van der Eycken, J.; Vandewalle, M. *J. Chem. Soc., Chem. Commun.* **1985**, 1719 and Van der Eycken, E.; De Bruyn, A.; Van der Eycken, J.; Callant, P.; Vandewalle, M. *Tetrahedron* **1986**, *42*, 5385.

(3) Lal, K.; Zarate, E. A.; Youngs, W. J.; Salomon, R. G. *J. Org. Chem.*, first of three papers in this issue.

(4) (a) Allinger, N. Quantum Chemistry Program Exchange, Program No. MMPX (85). (b) Clark, T. *A Handbook of Computational Chemistry*; Wiley-Interscience: New York, 1985. (c) Kao, J.; Allinger, N. L. *J. Am. Chem. Soc.* **1977**, *99*, 975.

0022-3263/88/1953-3688$01.50/0

Table I. Starting Dihedral Angles of the Dihydropyran Ring for XT

conformer	description	4,4a,8a,1	4a,8a,1,2	8a,1,2,3	1,2,3,4	2,3,4,4a	3,4,4a,8a
XT_{ee}	eq envelope	0	45	−60	60	−45	0
XT_{ae}	ax envelope	0	−45	60	−60	45	0
XT_{eb}	eq boat	0	−60	60	0	−60	60
XT_{ab}	ax boat	0	60	−60	0	60	−60
XT_{hc1}	half-chair	0	−30	60	−60	30	−30
XT_{hc2}	half-chair	0	30	−60	60	−30	30

[a] Looking down the bond formed by the center two atoms in the order given, if rotation of the front bond into the rear bond is clockwise, the angle value (in degrees) is positive. This convention is depicted for a 3,4,4a,8a dihedral angle of −30°:

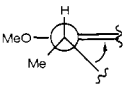

separation. Several approximations were made to simplify the calculations. The isobutyl moiety of 1 was replaced with a methyl group, and the methoxy substituents were held rigidly in the plane of the aryl ring with the methoxy methyls in an anti configuration relative to the pyran ring, but the methoxy carbon was allowed to rotate to minimize unfavorable interactions of the methyl hydrogens. These four diastereomers are designated XT, XC, NT, and NC, where X and N refer to an exo or endo configuration of the oxygen substituent on the camphane moiety and T and C refer to a trans or cis relationship between the quaternary carbon 3′ (in the camphane moiety) and the methyl substituent on position 4 of the dihydropyran ring. Only

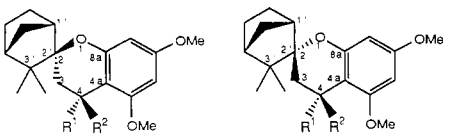

XT, $R^1 = CH_3$, $R^2 = H$ **NT**, $R^1 = H$, $R^2 = CH_3$
XC, $R^1 = H$, $R^2 = CH_3$ **NC**, $R^1 = CH_3$, $R^2 = H$

eight conformers of the benzodihydropyran ring were presumed potentially stable for each diastereomer: two boats, two half-chairs, and four envelope conformers. Detailed scrutiny revealed that two envelope conformers (with the pyran methylene carbon as the flap of the envelope) of each diastereomer are clearly unfavorable sterically (Figure 1). Thus, for each diastereomer two such conformers are possible, one with the quaternary carbon 3′ (in the camphane moiety) equatorial, designated with a subscript e, and one with that carbon axial, designated with a subscript a. Conformers XT_e and NT_e have an unfavorable 1,3-diaxial interaction between a methyl group and the bridgehead hydrogen atom at position 1′ of the camphane moiety. Conformers XT_a and NT_a have a less severe 1,3-diaxial interaction between a tertiary alkyl substituent and hydrogen but also a 1,3-peri interaction between a methoxy oxygen on the aromatic ring and the methyl group on the pyran ring. Similarly for diastereomers XC and NC, the envelope conformers XC_e and NC_e are destabilized by unfavorable 1,3-diaxial and 1,3-peri interactions. The conformers XC_a and NC_a incorporate a severe 1,3-diaxial interaction between a tertiary alkyl substituent and a methyl group.

Except for the pyran ring, all bond lengths, bond angles, and torsional angles were the same in the starting geometries for the remaining six conformers of each diastereomer. Starting geometries for the pyran ring of each conformer were set as exemplified (Table I) for diastereomer XT. These structures were energetically minimized by using the MMP2 program (see Experimental Section). The remaining six starting geometries for diastereomer XT converged on only four local minima XT_1–XT_4 (Figure 2). The half-chair and envelope starting geometries converged

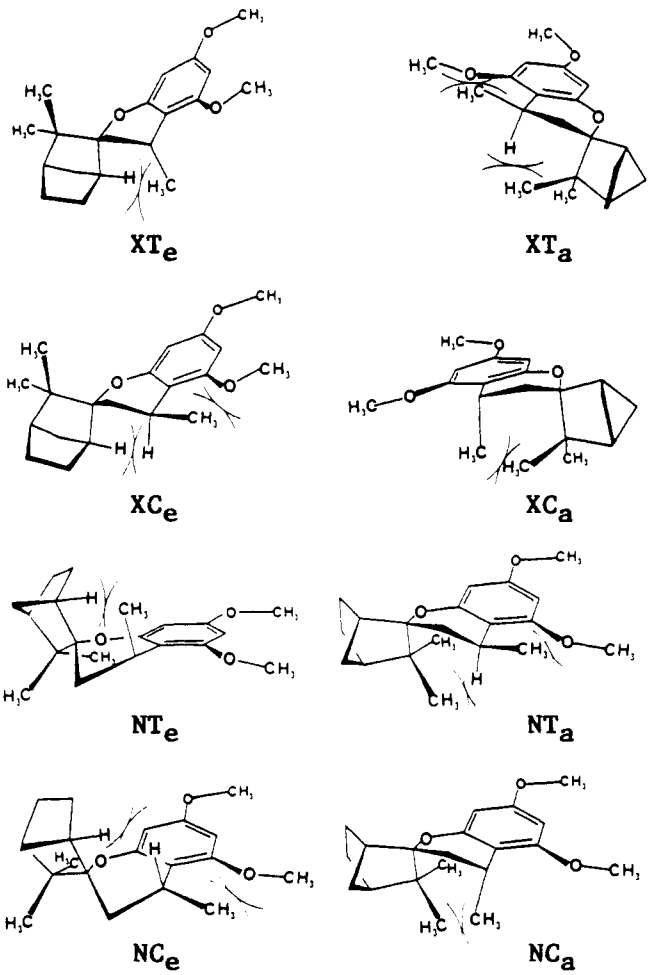

Figure 1. Unfavorable steric interactions in conformers involving the pyran methylene as the flap of an envelope.

on nearly ideal (Table I) envelope conformations. Thus, both XT_{hc1} and XT_{ae} converged on almost identical local minimum conformers XT_2 and $XT_{2'}$. Similarly, XT_{hc2} and XT_{ee} converged on the global minimum conformer XT_1. The two higher energy conformers of diastereomer XT resemble boats (Figure 2). However, comparison of the dihedral angles for idealized boat conformers (Table I) with those found for XT_3 and XT_4 (Table II) reveals major distortions. Especially noteworthy is the energetic proximity of the two lowest energy conformers of diastereomer XT. Separated by only 0.8 kcal/mol, these conformers should readily interconvert at room temperature (vide infra).

The other diastereomer with an exo configuration of the oxygen substituent on the camphane moiety, XC, also has two envelope conformers. Conformer XC_1 with the qua-

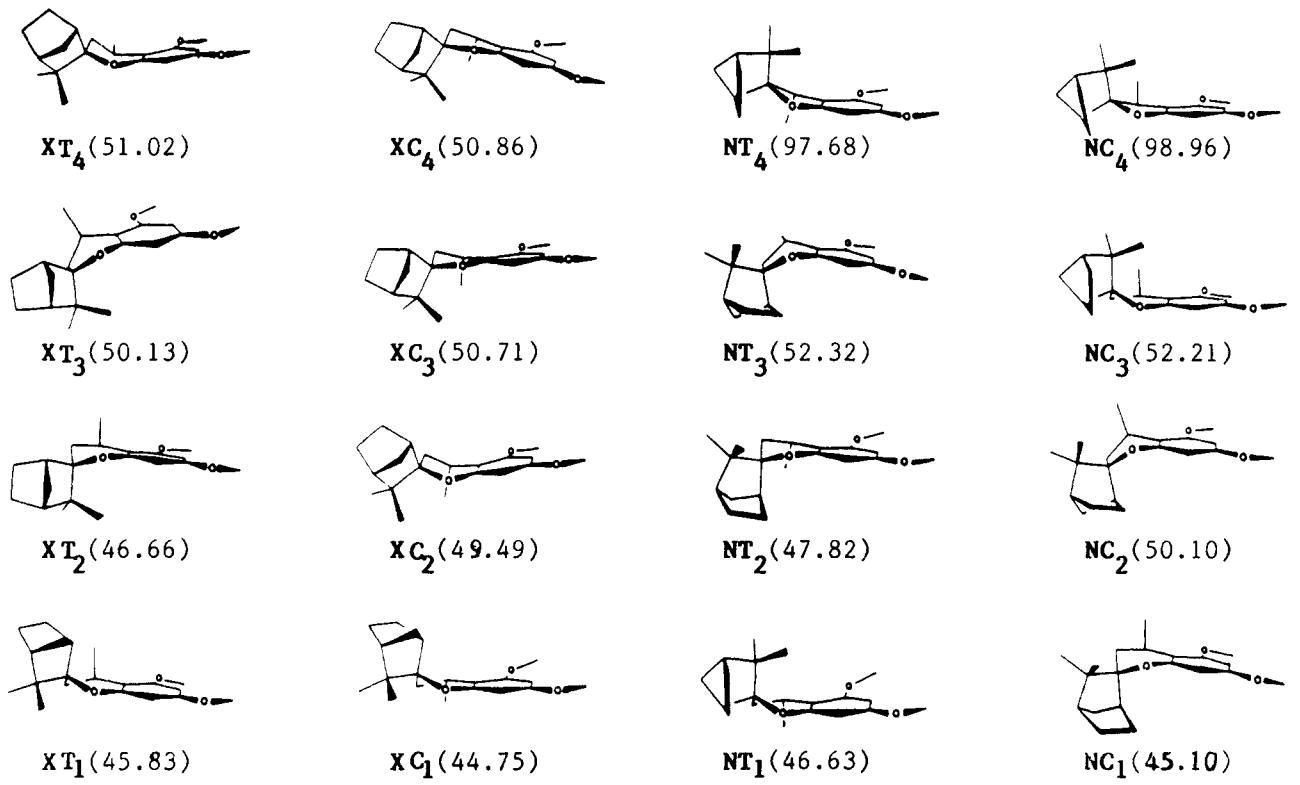

Figure 2. Four conformers of each diastereomer XT, XC, NT, and NC (steric energy, kcal/mol).

Table II. Dihedral Angles for the Dihydropyran Ring and Steric Energies Calculated for All Conformers of XT, XC, NT, and NC Found as Local Energy Minima by MMP2 Calculations with Six Starting Geometries for Each Diastereomer

start geometry[a]	conformer[a]	dihedral angle, deg						steric energy,[b] kcal/mol
		4,4a,8a,1	4a,8a,1,2	8a,1,2,3	1,2,3,4	2,3,4,4a	3,4,4a,8a	
ee, hc2	NC_1 (ee)	-5.3	-26.0	56.7	-60.3	32.6	0.2	45.10
eb	NC_2 (eb)	-1.0	-47.9	43.1	4.2	-45.6	44.8	50.10
ae, hc1	NC_3 (ae)	3.2	26.1	-50.5	50.7	-25.7	-1.9	52.21
ab	NC_4	1.0	29.5	36.3	19.4	5.3	-16.0	98.96
ae, hc1	NT_1 (ae)	6.8	24.8	-54.2	57.0	-29.5	-2.5	46.63
ee	NT_2 (ee)	-2.4	-22.9	50.1	-57.3	35.3	-5.1	47.82
eb	NT_3 (eb)	-1.5	-51.4	45.4	6.2	-51.4	49.4	52.32
ab	NT_4	3.0	33.3	-39.8	16.7	12.8	-23.2	97.68
hc2	NT_5	-1.0	26.6	-41.8	36.9	-12.4	-7.7	138.33
ee, hc2	XC_1 (ee)	5.4	20.8	-53.3	63.4	-40.2	5.9	44.75
eb	XC_2 (deb)	0.4	35.1	-21.1	-23.5	53.0	41.2	49.49
hc1	XC_3	1.9	-4.6	25.3	-45.5	43.4	-20.8	50.71
ae, ab	XC_4 (dae)	0.5	-15.0	37.5	-49.2	37.3	-12.1	50.86
ee, hc2	XT_1 (ee)	2.4	21.8	-50.5	59.9	-38.9	7.4	45.83
hc1	$XT_{2'}$ (ae)	-7.4	-24.2	54.4	-57.4	29.9	2.7	46.65
ae	XT_2 (ae)	-6.7	-22.3	52.1	-57.4	32.3	-0.1	46.66
ab	XT_3 (dab)	-0.5	-37.0	22.1	24.9	-56.0	43.3	50.13
eb	XT_4 (deb)	0.1	36.6	-17.3	-33.1	64.0	-46.7	51.02

[a] The designations ae, ee, ab, eb, hc1, and hc2 indicate conformations that are approximately described as axial envelope, equatorial envelope, axial boat, equatorial boat, half-chain 1, and half-chair 2 as defined in Table I for the starting geometries of the dihydropyran ring. The designations deb, dab, and dae indicate conformations that are distorted equatorial boat, axial boat, and axial envelope respectively [b] The "corrected steric energy" as defined in ref 4c.

ternary carbon 3′ in the camphane moiety equatorial on the dihydropyran ring corresponds to the global minimum energy conformation. However, in contrast with diastereomer XT, the other envelope conformer of XC is not at all energetically similar to the global minimum. An unfavorable steric interaction between the methyl and tertiary alkyl substituents on the dihydropyran ring raises the energy of the other (distorted) envelope conformer XC_4 above that of XC_2, a distorted boat, and XC_3. Most importantly, the two lowest energy conformers of diastereomer XC_2 are separated by more than 4.7 kcal/mol. In contrast with its conformationally mobile epimer XT, XC is predicted to be locked in the XC_1 conformation at room temperature. It would be wrong to presume that the structures depicted in Figure 2 are necessarily the four lowest energy conformers for each diastereomer since the starting geometries presented in Figure 1 were not energetically minimized. It seems likely however that all possible lower energy conformers were found since the identification of candidate starting geometries by examination of molecular models is straightforward for simple structures such as six-membered rings.[5]

(5) This procedure was used previously to define reasonable starting geometries for conformers: Bowen, P.; Allinger, N. L. *J. Org. Chem.* **1986**, *51*, 1513.

A similar dichotomy was found between the two diastereomers NT and NC with endo configurations of the oxygen substituent on the camphane moiety. As for the diastereomers XT and XC, the global energy minimum conformers of NT and NC are envelopes, NT_1 and NC_1 respectively. For diastereomer NT, another envelope conformer, NT_2, is separated by only 1.2 kcal/mol from the global minimum, and these conformers should readily interconvert at room temperature. However, for diastereomer NC the energy of a second envelope conformer, NC_3, is raised above that for a boat conformer NC_2 by an unfavorable steric interaction between the methyl and tertiary alkyl substituents on the dihydropyran ring. In contrast with NT, the two lowest energy conformers of NC are separated by 5.0 kcal/mol, and diastereomer NC is predicted to be locked in the NC_1 conformation at room temperature. In summary, XC and NC are predicted to be locked in conformations XC_1 and NC_1 respectively while XT and NT are expected to exist as mixtures of conformers XT_1 plus XT_2 and NT_1 plus NT_2 respectively.

Variable-Temperature ^{1}H NMR Spectra. The exo configuration of the diastereomers **1xc** and **1xt** and the endo configuration of the diastereomers **1nt** and **1nc** at the spiro junction are firmly established by synthesis from the ketones *exo*-**2** and *endo*-**2** respectively.[1] Determination

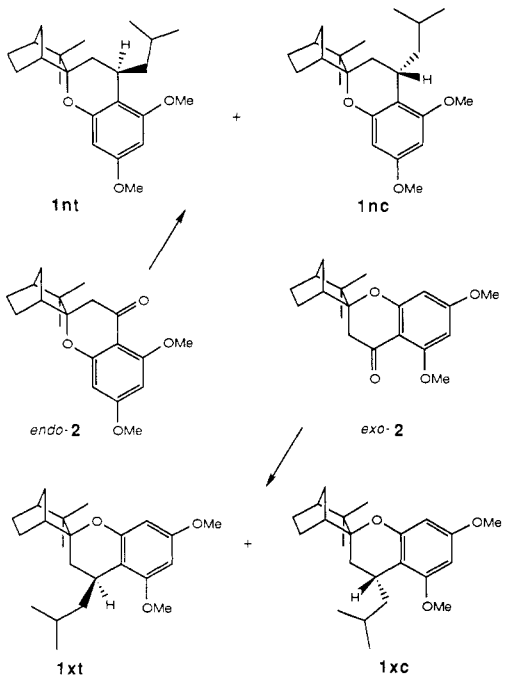

of the relative configurations for each benzylic epimer is a difficult problem. The results of MMP2 calculations outlined above suggest that the relative configurations of epimers at position 4 in the dihydropyran ring should be differentiable by variable-temperature ^{1}H NMR studies. Conformational mobility is expected for diastereomers **1xt** and **1nt** but not for **1xc** and **1nc** in analogy with the model compounds in Figure 2. Of the epimeric exo diastereomers, the ^{1}H NMR spectrum of the conformationally mobile epimer **1xt** should change as conformer populations change appreciably with temperature while the ^{1}H NMR spectrum of the rigid epimer **1xc** should be less temperature dependent.

The upfield methyl resonances in ^{1}H NMR spectra at −21 and 70 °C of the epimeric exo diastereomers **1xt** and **1xc** presented in Figures 3A and 3B respectively show the predicted temperature dependence. Only one methyl singlet resonance shifts substantially with temperature

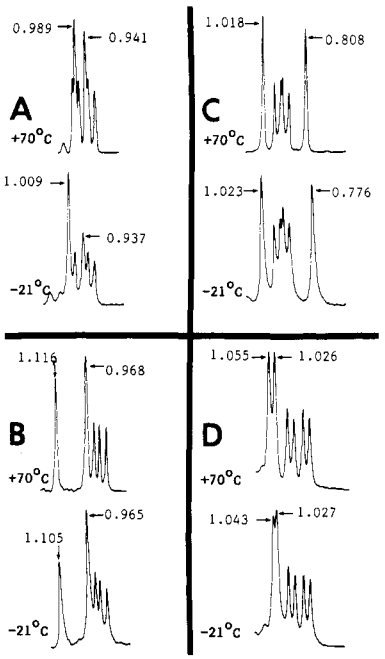

Figure 3. Isopropyl and camphane moiety methyl resonances in the ^{1}H NMR spectra of (A) **1xt**, (B) **1xc**, (C) **1nt**, and (D) **1nc** at −21 and 70 °C.

change. The shift is twice as great for one epimer (Figure 3A), now assigned structure **1xt**, than for the other (Figure 3B), now assigned structure **1xc**. The direction of the chemical shift change, upfield with increased temperature, is also noteworthy. Two energetically similar envelope conformers, analogous to XT_1 and XT_2 (Figure 2), are expected for **1xt**. Presuming a Boltzmann distribution of **1xt** over the two conformations which differ in energy by only ΔE = 0.83 kcal/mol, the population of the higher energy conformer would change from 23% to 46% with a temperature increase from −21 to 70 °C assuming that $\Delta G = \Delta E + T\Delta S_{mix}$ and applying the thermodynamic equation $\Delta G = -RT \ln K$ and $\Delta S_{mix} = R\sum_i N_i \ln N_i$ where ΔS_{mix} is the entropy of mixing and N_i is the mole fraction of each component conformer in the equilibrium mixture.[6] Consideration of the structures of XT_2 and XT_1 (Figure 2) suggests that such a shift in conformer populations for **1xt** would result in an upfield shift of the resonance corresponding to the exo methyl group since its average environment would include a greater proportion of a conformer resembling XT_2 in which the exo methyl group is more strongly shielded owing to greater proximity to the paramagnetic shielding region over the aromatic ring than in the lower energy conformer resembling XT_1.

A more quantitative analysis of the shielding influence of the aromatic π electrons in XT on the hydrogens of the exo and endo methyl groups in the camphane moiety of XT_1 and XT_2 was also performed. The spatial relationship between these hydrogens and the aromatic ring was defined in terms of elevation above the plane of the ring (z axis) and horizontal distance from the center of the ring (p axis). These distances and the predicted[7] shielding (−) or deshielding (+) influence of the aromatic electrons upon each hydrogen are presented in Table III for the two lowest

(6) Eliel, E. L.; Allinger, N. L.; Angyal, S. J.; Morrison, G. A. *Conformational Analysis*; American Chemical Society: Washington, DC, 1981; p 24.

(7) (a) Ensley, J. W.; Feeney, J.; Sutcliffe, L. H. *High Resolution Nuclear Magnetic Resonance Spectroscopy*; Pergamon: New York, 1965; Vol. 1, pp 595–604. (b) Johnson, C. E.; Bowey, F. A. *J. Chem. Phys.* **1958**, *29*, 1012.

Table III. Location of Hydrogen Nuclei in the Methyl Groups of the Camphane Moiety of XT and NT Relative to the Aromatic Ring and Consequent Paramagnetic Shielding (-) or Deshielding (+)

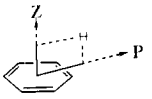

	exo methyl			endo methyl		
		distance[b]			distance[b]	
conformer	shielding (av)[a]	p axis	z axis	shielding (av)[a]	p axis	z axis
XT_1	0.14	3.55	1.07	>0.12	4.23	0.96
	>0.15	4.63	0.37	>0.16	4.55	0.15
	0.20	3.65	0.01	>0.16	5.10	0.15
	(>0.16)			(>0.15)		
XT_2	-0.30	1.76	2.87	-0.09	2.81	2.92
	-1.40	0.95	1.89	-0.17	2.22	2.08
	-0.14	2.05	1.83	0.06	3.37	1.83
	(-0.61)			(-0.07)		
NT_1	0.06	2.37	1.90	-0.33	1.70	2.87
	-0.12	2.56	2.93	-0.13	2.16	1.86
	-0.19	2.11	1.96	-1.54	0.98	1.81
	(-0.08)			(-0.67)		
NT_2	>0.16	4.58	0.02	>0.16	4.66	0.26
	>0.15	5.06	0.37	0.22	3.63	0.03
	>0.17	3.33	1.07	0.15	3.64	1.05
	(>0.16)			(>0.17)		

[a] Shielding values calculated by using tables from ref 7a with units of parts per million; values in parentheses are for shielding in the average environment of the hydrogens of each methyl group. [b] Units are ring radii = 1.39 Å.

energy conformers of XT and NT. In conformer XT_1 the hydrogens of the exo methyl group experience a slight deshielding (>0.16 ppm) owing to the paramagnetic effect of the aromatic π electrons while these same hydrogens are strongly shielded (-0.56 ppm) in conformer XT_2. At higher temperatures, where the proportion of the XT_2 conformer is greater, the resonance for the exo methyl hydrogens should appear at higher field than at lower temperature where the proportion of the XT_2 conformer is less. In contrast, little change in the chemical shift of the endo methyl hydrogens is predicted as a result of changes in the proportions of these conformers. The temperature dependence of the ^1H NMR spectra of the epimeric exo diastereomers (Figure 3) corresponds with predictions except for the small changes observed in the ^1H NMR spectrum of **1xc**. Since the latter epimer is predicted to be conformationally rigid, no variation of chemical shift with temperature is expected. Obviously, factors other than changes in the orientation of the aromatic π electrons contribute to the temperature-dependent changes in the chemical shifts observed. Our analysis also leads to the conclusion that the lower field methyl singlet in Figure 3A corresponds to the exo methyl group in **1xt**.

A similar analysis of the shielding influence of the aromatic π electrons on the hydrogens of the exo and endo methyl groups in the camphane moiety of NT_1 and NT_2 leads to the conclusion that the ^1H NMR resonance for the endo methyl group hydrogens in **1nt** will shift to lower field with increasing temperature. Thus, presuming a Boltzmann distribution of **1nt** over the two conformations which differ in energy by only $\Delta E = 1.19$ kcal/mol, the population of the higher energy conformer would change from 11% to 21% with a temperature increase from -21 to 70 °C. This increase in the proportion of the higher energy conformer analogous to NT_2, where these hydrogens are weakly deshielded (>0.17 ppm), and a decrease of the lower energy conformer analogous to NT_1, where these hydrogens are strongly shielded (-0.67 ppm), will result in net deshielding in the average environment of the endo methyl group. In contrast, little change in the chemical shift of the exo methyl hydrogens is predicted as a result of changes in the proportions of these conformers.

The upfield methyl resonances in ^1H NMR spectra at -21 and 70 °C of the epimeric endo diastereomers **1nt** and **1nc** presented in Figures 3C and 3D respectively clearly show the predicted temperature dependence. Only one methyl singlet resonance shifts substantially with temperature change (Figure 3), the upfield singlet in Figure 3C. The epimer corresponding to Figure 3C is, therefore, now assigned the structure **1nt** while that corresponding to Figure 3D is now assigned structure **1nc**. The direction of the chemical shift change, downfield with increased temperature, is also noteworthy because it contrasts with the behavior of the exo epimer **1xt** and because it agrees with the quantitative predictions outlined above. This analysis also leads to the conclusion that the higher field methyl singlet in Figure 3C corresponds to the endo methyl in **1nt**.

Nuclear Overhauser Effects. NOE experiments[8] independently confirm the stereostructural conclusions of the previous section. The ^1H NMR spectra of the diastereomers of **1** are generally complex. Most resonances overlap with other resonances, making it difficult to unambiguously irradiate a specific resonance or to measure the consequent effects on other specific resonances. The most unambiguous and, thus, most reliable NOE experiments involve effects produced between *isolated* resonances. Two resonances that are *isolated* in the spectrum of every diastereomer of **1** are those for the bridgehead hydrogen at position 1′ in the camphane moiety and the benzylic hydrogen at position 4 in the dihydropyran moiety. In the narrow line approximation for like nuclei with spin $^1/_2$, nuclear Overhauser enhancements are proportional to r^{-6}, where r is the internuclear distance between the interacting nuclei.[9] The internuclear distance between these hydrogen atoms in each conformer shown

(8) (a) Sanders, J. K. M.; Mersh, J. D. *Prog. Nucl. Magn. Reson. Spectrosc.* **1982**, *15*, 353-400. (b) Keller, T. H.; Neeland, E. G.; Weiler, L. *J. Org. Chem.* **1983**, *48*, 1870.

(9) (a) Saunders, J. K.; Easton, J. W. *Determination of Organic Structure by Physical Methods*; Nachad, F. C., Zuckerman, J. J., Randall, E. W., Eds.; Academic: New York, 1976; Vol. 6. (b) Schirmer, R. E.; Noggle, J. H.; Davis, J. P.; Hart, P. A. *J. Am. Chem. Soc.* **1970**, *92*, 3266. (c) Bell, R. A.; Sanders, J. K. *Can. J. Chem.* **1970**, *48*, 1114.

Table IV. Internuclear Distance between the Bridgehead and Benzylic Hydrogens

conformer	distance, Å	conformer	distance, Å
XT_1	4.187	NT_1	4.732
XT_2	5.014	NT_2	3.997
XT_3	4.388	NT_3	4.454
XT_4	4.675	NT_4	4.814
XC_1	2.596	NC_1	2.332
XC_2	4.647	NC_2	4.198
XC_3	4.679	NC_3	4.440
XC_4	4.666	NC_4	4.088

Table V. Nuclear Overhauser Enhancements

	1xt	1nt	1xc	1nc
benzylic H[a]	<1.0	<1.0	5.8	7.6
bridgehead H[b]	<1.0	<1.0	5.7	9.4
predicted[c]	0.2	0.2	4.9	*c*

[a] Percent enhancement upon irradiation of the bridgehead hydrogen. [b] Percent enhancement upon irradiation of the benzylic hydrogen. [c] Setting NOE for **1nc** at 9.4% and assuming NOE $\propto r^{-6}$.

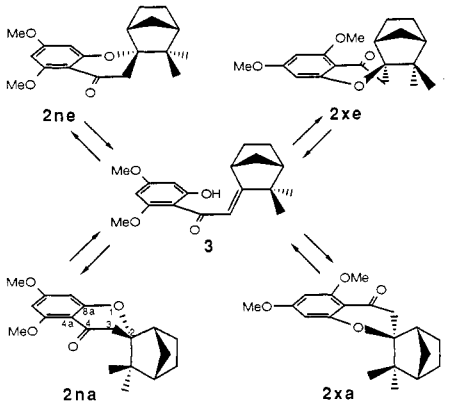

Figure 4. Equilibria between conformers of *exo*- and *endo*-**2** and enone **3**.

in Figure 2 was readily available from the energy-minimized structures produced by MMP2 calculations. These distances are listed in Table IV. Measurable enhancements are only predicted for two diastereomers, XC and NC. These diastereomers are locked in their envelope conformers XC_1 and NC_1. Since the internuclear distance in NC_1 is somewhat less than in XC_1, a larger enhancement is anticipated for NC than for XC. For the diastereomers of **1**, therefore, no enhancement is expected for **1xt** or **1nt** while some enhancement should be found for **1xc** and a greater enhancement is predicted for **1nc**. These predictions are nicely confirmed by experiment (Table V).

Configurational Equilibrium between Epimers. Our synthesis of the epimeric ketones *endo*-**2** and *exo*-**2** was achieved by a base-catalyzed intramolecular Michael addition of a phenol to an α,β-unsaturated ketone in the precursor **3**. This cyclization was highly stereoselective, favoring the exo adduct over its endo epimer by 95:5.[1] It seemed likely that this selectivity was kinetic in origin, arising from the well-known rate advantage for addition to the exo face of norbornyl derivatives. To explore another application of molecular mechanics calculations, we undertook prediction of the thermodynamic ratio of the epimeric dihydrobenzopyranones **2**. Examination of molecular models revealed that only two envelope conformers of each epimer were likely: one with the tertiary alkyl substituent on the pyranone ring axial, designated by **a** in **2xa** or **2na**, and one with that group equatorial, designated by **e** in **2ne** or **2xe** (Figure 4).

Table VI. Steric Energies Calculated for Isomers of 2 by Using Various Parameters

parameter set[a]	2xa	2xe	2na	2ne
A	48.38	47.74	47.95	47.50
B	48.38	47.76	47.86	47.43
C	45.35	44.96	47.14	46.42

[a] A: $V_1 = V_3 = 0$; $V_2 = 16.25$ kcal/mol (angle 4,4a,8a,1), $\mu = 1.5$. B: $V_1 = V_3 = 0$; $V_2 = 8.0$ kcal/mol (angle 4,4a,8a,1), $\mu = 1.5$. C: $V_1 = V_3 = 0$; $V_2 = 16.25$ kcal/mol (angle 4.4a,8a,1), $\mu = 32.63$.

Table VII. Composition of Mixtures of *endo*-2 and *exo*-2 at Equilibrium

parameter set	*endo*-2, %	*exo*-2, %
A	58	42
B	62	38
C	11	89
obsd	48	52

To simplify the calculations, we restricted the methoxy groups in all isomers of **2** to the plane of the aryl ring as described above for calculations on **1**. Torsional parameters for the 4,4a,8a,1 dihedral angle in, e.g., **2nx** (Figure 4) are not available in the MMP2 program. This connectivity was modeled, therefore, as a Csp^3–Csp^2–Csp^2–Csp^2 torsional angle, i.e., α,β-unsaturated carbonyl, for which the torsional parameters are available. Thus, the starting geometries were energetically minimized by using the torsional parameters $V_1 = V_3 = 0$ and $V_2 = 16.25$ kcal/mol and the default value $\mu = 1.5$ for the local dielectric (parameter set A). The calculated steric energies for the isomers of **3** are presented in Table VI.

The parameters used above for the 4,4a,8a,1 dihedral angle, e.g., in **2na** (Figure 4), modeled the aryl C–C bond as a double bond as in **4a**. However, it might be appropriate to use a lower torsional barrier for a C–C bond in an aromatic ring. Therefore the aryl C–C bond was assigned a lower torsional barrier (parameter set B) by reducing V_2 to half the value presumed above (i.e., $V_1 = V_3 = 0$, $V_2 = 8$ kcal/mol) since the resonance contributions possible in an aromatic system would allow more torsional movement around the 4,4a,8a,1 torsional angle, i.e., both structure **4a** with a 4a,8a C–C double bond and structure **4b** with a 4a,8a C–C single bond must be averaged.

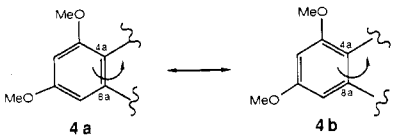

4a 4b

The above calculations presumed the MMP2 default value of 1.5 for the local dielectric constant (μ). However, this value is representative of the gas phase. Therefore, starting geometries were minimized with $V_1 = V_3 = 0$, $V_2 = 16.25$ kcal/mol, and $\mu = 32.63$ (parameter set C), since 32.63 is the bulk dielectric constant of methanol, a reasonable analogy for the solvent used for equilibration (vide infra), a 1:9 mixture of water and ethanol. We recognize that the bulk dielectric of the media is not expected to be identical with the local dielectric, which, however, is not readily available.[10]

Equilibrium compositions of *exo*-**2** = **2xa** + **2xe** and *endo*-**2** = **2na** + **2ne** epimers were calculated at 80 °C for each parameter set (see Table VII) by using the thermodynamic equation $\Delta G_{ep} = -RT \ln K_{ep}$ where ΔG_{ep} is the free energy change associated with interconversion of the

(10) Allinger, N. L. *Operating Instructions for* MM2 *and* MMP2 *Programs*; Quantum Chemistry Program Exchange, Indiana University (Department of Chemistry): Bloomington, IN, 1985; p 58.

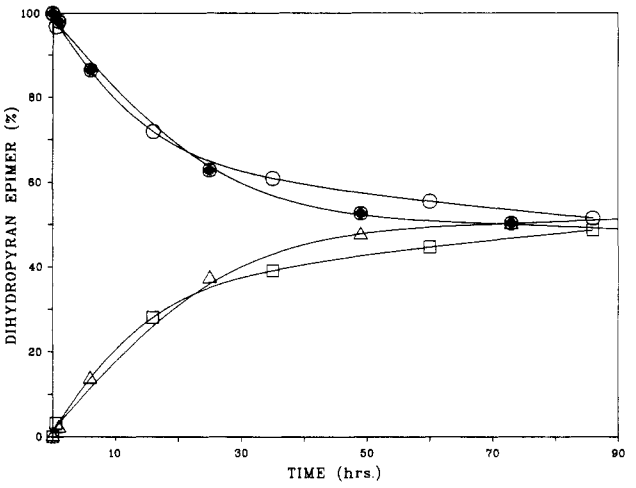

Figure 5. Equilibration of pure *exo*-**2** to exo (○) and endo (□) epimers or pure *endo*-**2** to endo (●) and exo (△) epimers.

endo and exo epimers and K_{ep} is the equilibrium constant for this epimerization. That is, $\Delta G_{ep} = \Delta G_x - \Delta G_n$. Furthermore, $\Delta G_x = \Delta H_x - T\Delta S_x$ where ΔG_x is the free energy, ΔH_x is the enthalpy, and ΔS_x is the entropy of mixing (the conformers) of the exo epimer, and ΔG_n is defined similarly for the endo epimer. Therefore, $\Delta G_{ep} = \Delta H_x - \Delta H_n - T(\Delta S_x - \Delta S_n)$. Since MMP2 defines $\Delta H_x = SE_x + 4RT + BE_x$ and $\Delta H_n = SE_n + 4RT + BE_n$,[11] and since $BE_x = BE_n$ for epimers, $\Delta G_{ep} = SE_x - SE_n - T(\Delta S_x - \Delta S_n)$ where BE_i is the bond energy and SE_i the steric energy of a molecule. The steric energy for the epimer *exo*-**2** was calculated from the steric energies SE_{xa} and SE_{xe} of its conformers **2xa** and **2xe** (see Table VI) by using the equation $SE_x = \sum_i N_i SE_i$ where N_i is the mole fraction of each conformer, i.e., $N_{xe} + N_{xa} = 1$. The mole fractions N_{xe} and N_{xa} of the equatorial and axial conformers **2xe** and **2xa** were calculated by using the equation $K_x = e^{-(SE_{xe}-SE_{ne})/RT} = N_{xe}/N_{xa}$ where K_x is the equilibrium constant for the conformers of the epimer *exo*-**2** on the assumption that the various conformations are equal in entropy.[6] ΔS_x, the entropy of mixing the conformers of *exo*-**2**, was determined from the equation $\Delta S_x = -R\sum_i N_i \ln N_i$.[6]

Comparison of the results obtained with parameter sets A and B (Table VII) shows that the choice of torsional parameter for the 4a,8a C–C bond in the aromatic ring of **2** has only a small effect on the equilibrium ratio predicted for the endo and exo epimers. Comparison of the equilibrium ratios calculated with parameter sets A and C (Table VII) shows that the change from a nonpolar to a very polar environment shifts the equilibrium from a slight preference for *endo*-**2** to a preference for *exo*-**2**. Therefore, either the 95:5 preference for the exo epimer found for base-catalyzed cyclization of enone **3** is kinetic in origin, or the MMP2 default value $\mu = 1.5$ grossly underestimates the local dielectric constant.

Epimerization of pure *endo*- or *exo*-**2** to an equilibrium mixture was achieved upon boiling a solution in 10% aqueous ethanolic potassium carbonate for 90 h (Figure 5). This interconversion proceeds through the acylic enone intermediate **3** (see Figure 4), traces of which were also detected in these reaction mixtures. The ratio of *exo*- to *endo*-**2**, 52:48, observed at equilibrium agrees remarkably well with the ratio calculated by MMP2 using the default value for $\mu = 1.5$ in spite of the uncertainty regarding a torsional parameter and the simplification of restricting the aryl methoxy substituents to the plane of the aromatic ring, ignoring the rotational entropy of the methoxy groups. The errors introduced by the approximations used most likely cancel since differences in the steric energies of epimers are considered instead of their absolute values.

Experimental Section

Calculations. Starting geometries for energy minimizations with the MMP2 program (QCPE; Bloomington, IN)[10] were chosen by examining molecular models and choosing reasonable conformations.[5] For each diastereomer, coordinates for one of the starting geometries in Table I were generated graphically by using a VAX-11/785 (Digital Equipment Corp.) computer with a Lundy-68X (Lundy Electronics and Systems, Inc.; Glenhead, NY) terminal in the DRAWMOL subprogram of the Chemlab-II V8.0[12] program. This generated a two-dimensional set of coordinates for the molecule, which was then submitted to the PRXBLD subprogram[13] of Chemlab-II to generate a three-dimensional set of coordinates (mol file). The mol file was energetically minimized by using MMP2 with the methoxy groups of the aryl ring fixed anti to the dihydropyran ring and in the plane of the aryl ring and the methyl of the methoxy group allowed to rotate freely. For all remaining starting geometries, the set of coordinates for the energetically minimized geometry was transferred to the ChemGraf[14] program, and the dihedral angles of the dihydropyran ring were set to the starting values listed in Table I, all the other bond lengths and angles being kept the same as found for the minimized geometry. The five remaining starting geometries so generated for each diastereomer were then minimized. The coordinates of the local energy minimum conformations obtained were then plotted in the SPACFIL subprogram of Chemlab-II after orienting the mol file (i.e., choosing an informative projection) by using the ChemGraf program. Coordinates for all of these conformers can be reproduced readily from the coordinates of the lowest energy conformation of each diastereomer by adjusting the dihedral angles to the appropriate values (Table II), keeping all other bond lengths and angles the same, and energy minimizing the resulting starting geometries with MMP2.

Coordinates for starting geometries of conformers of *endo*- and *exo*-**2** were generated in an analogous manner. In this case, the O sp^3–Ar sp^2–carbonyl sp^2 torsional angle was set at $V_1 = V_3 = 0$ and $V_2 = 16.25$ or 8.0 kcal/mol. The dieletric constant was set at either 32.63 or the default value (1.5).

Nuclear Overhauser Effects. NOE experiments were performed with a Bruker 400 MSL instrument. A presaturation program was used, which gave a 7-s presaturation pulse followed by a 2.5-s acquisition time. The decoupling power was set at the minimum power required to cause disappearance of the resonance being irradiated. Difference spectra were obtained by alternating sets of acquisitions with the decoupler frequency set to that of the resonance of interest for four acquisitions and then to −10 000 Hz for four acquisitions. This sequence was followed to accumulate 16 transients for each spectrum. The two spectra were then subtracted, and the NOE was measured as the percent intensity difference with the $CHCl_3$ resonance set to zero intensity difference as an internal standard. The spectra were acquired in $CDCl_3$, which had been saturated with argon immediately before the experiment, at concentrations of 35 mM for each isomer at ambient temperature. Intraproton distances, d, were calculated from the coordinates of the protons of interest located in the mol file (the data file containing the Cartesian coordinates) by using $d = [(x_1 - x_2)^2 + (y_1 - y_2)^2 + (z_1 - z_2)^2]^{1/2}$.

Variable-Temperature ^{1}H NMR. The instrument used was a 200-MHz Varian XL-200H. Each sample contained 3 mg of compound/mL of CCl_4, and the shifts were measured relative to internal TMS. Samples were allowed to thermally equilibrate in the probe for 5–10 min prior to the start of each experiment.

(11) Burket, U.; Allinger, N. L. *Molecular Mechanics*; ACS Monograph 177; American Chemical Society: Washington, DC, 1982; p 174.

(12) Pearlstein, R. A. "*CHEMLAB-II*" *REVISION 8.0* (by Toni Childress); Molecular Design Limited: San Leandro, CA 1985. For the molecular modelling software system developed under the direction of Dr. A. J. Hopfinger of Chemlab, Inc.

(13) Wipke, T. D. *PRXBLD*, revision 5.0 (by Toni Childress); Molecular Design Limited: Hayward, CA, 1984.

(14) Davies, E. K. (Chemical Crystallography Laboratory, Oxford University) *ChemGraf*; Chemical Design Ltd.: Oxford, England, 1985.

Temperatures were read from the instrument panel and were constant within ±0.2 °C during each experiment. All spectra were plotted at 1500 Hz/50 cm. Chemical shifts of the hydrogens of the geminal methyl groups for each diastereomer at −21 and 70 °C are given in Figure 3.

For predictions of paramagnetic shielding or deshielding of hydrogens in the geminal methyl groups in XT_1, XT_2, NT_1, and NT_2 (data presented in Table III), the Cartesian coordinates of the mol file were transposed into cylindrical coordinates. The cylindrical z axis is normal to the plane of the aromatic ring with its origin at the center of the ring. The p axis is in the plane of the aromatic ring with its origin at the center of the ring. The molecule was first oriented with one carbon of the aromatic ring at the origin (e.g., atom 4a), a vicinal carbon of the aromatic ring on the positive Cartesian z axis (e.g., atom 8a), and a third carbon of the aromatic ring on the positive Cartesian y axis (e.g., atom 6), using the ALIGN command in the ORIENT subprogram of Chemlab-II. The Cartesian x axis is thus normal to the aromatic

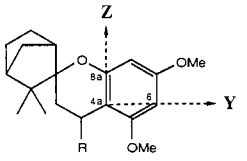

ring, and the cylindrical z coordinate will correspond to the Cartesian x coordinate of any atom in the molecule thus oriented. The y and z Cartesian coordinates for the center of the aromatic ring are then $y/2$ and $z/2$ for the ring atoms located on the y and z axes respectively (e.g., atoms 6 and 8a). The cylindrical p coordinate for any atom whose Cartesian coordinates are x_n,y_n, z_n is then computed from the relationship $p = [(y_n - y/2)^2 + (z_n - z/2)^2]^{1/2}$.

Equilibration of Dihydropyranones *endo*-2 and *exo*-2. Ketone *endo*-**2** (0.130 g, 0.41 mmol) and anhydrous potassium carbonate (1.2 g) in 90% ethanol (59 mL) were heated at reflux under nitrogen. After 1.0, 6.0, 25.0, 49.0, 73.0, 121.0, 170.0, and 219.0 h, aliquots (2–3 mL) were removed from the reaction mixture and diluted with methylene chloride (10 mL). These were washed with water, dried ($MgSO_4$), and stripped of volatiles under reduced pressure to yield samples for subsequent ^1H NMR ($CDCl_3$) analysis. The isomeric ratio was determined by integration of an expanded plot of the region (490–805 Hz). After 219 h, 9% of the α,β-unsaturated ketone **3** was present as determined by comparison of integral peak areas of the signal at δ 6.66 (1 H, s) for the vinyl hydrogen of **3** to that of the resonances for the hydrogens of the methylene α to the carbonyl group for *exo*-**2** at δ 2.70 (H, d, J = 16.2 Hz) and 2.72 (H, d, J = 16.2 Hz) and for *endo*-**2** at δ 2.53 (H, d, J = 16.2 Hz) and 2.83 (H, d, J = 16.2 Hz). The integral peak areas for the above-mentioned methylene hydrogen resonances were compared to give the ratio of *exo*-**2** to *endo*-**2** in each aliquot. The isomerization of *exo*-**2** to an equilibrium mixture of *exo*- and *endo*-**2** was carried out similarly.

Acknowledgment. This work was supported by a grant from the National Science Foundation. We thank Prof. Gilles Klopman for access to his ChemGraph and Chemlab programs.

Registry No. **1nt**, 114976-79-3; **1nc**, 114906-85-3; **1xt**, 114906-84-2; **1xc**, 114976-78-2; *endo*-**2**, 114906-86-4; *exo*-**2**, 114976-80-6; **3**, 114906-87-5; **XT**, 114906-88-6; **XC**, 114976-81-7; **NT**, 114976-82-8; **NC**, 114976-83-9.

On the Photobiology of the Gilvocarcins. Total Synthesis of Defucogilvocarcin V and a Related Photoactive Vinyl Phenol[1]

Lawrence R. McGee* and Pat N. Confalone

Central Research and Development Department, E. I. du Pont de Nemours and Co. Inc., Experimental Station, Wilmington, Delaware 19898

Received January 13, 1988

Defucogilvocarcin V (**4a**) and the related vinyl phenol **5a** are important for the study of the photonicking of DNA by gilvocarcin antibiotics such as 1. They have been synthesized from a common precursor, lactone **6a**, which contains the complete carbon framework, prepared in the first step. Key transformations include introduction of functionality at C-10 by a regiospecific selenium dioxide oxidation and at C-12 by Fremy's salt oxidation of the phenol function hidden in ring C. The vinyl group is introduced by sequential radical bromination–dehydrobromination. These vinyl phenols photonick DNA under the same conditions as the natural glucoside 1 and serve as bioorganic tools in the study of the mechanism of the nicking reaction.

Gilvocarcin V[2,3] (1) represents a new class of aromatic *C*-glycoside antibiotics with significant antitumor activity.

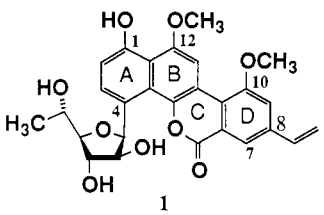

1

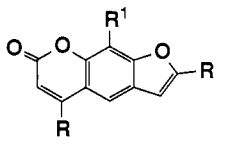

2: R=CH_3-, R^1=CH_3O-
3: R=CH_3-, R^1=CH_3-

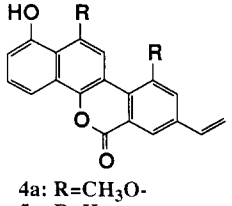

4a: R=CH_3O-
5a: R=H-

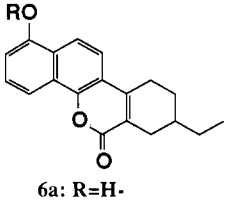

6a: R=H-

The in vitro activity of these molecules is dependent upon activation by low-energy light.[4] In contrast to the photoactive psoralens such as 8-methoxypsoralen (8-MOP) (**2**), and trioxsalen (**3**) which covalently modify or cross-link duplex DNA,[5] the gilvocarcins cause single-strand breaks in double-stranded DNA upon irradiation.[6] Experimen-

(1) Contribution no. 4206. Presented at the 191st National Meeting of the American Chemical Society, New York, NY, April 1986; paper ORGN 195.

(2) Takahashi, K.; Yoshida, M.; Tomita, F.; Shirahata, K. *J. Antibiot.* **1981**, *34*, 271–275.

(3) Toromycin (Horii, S.; Fukase, H.; Mizuta, E.; Hatano, K.; Mizuno, K. *Chem. Pharm. Bull.* **1980**, *28*, 3601–3611) and anandimycin (Balitz, D. M.; Bush, J. A.; O'Herron, F. A.; Nettleton, D. E., Jr. U.S. Patent 4 360 595) are other names for gilvocarcin.

(4) Elespuru, R. K.; Gonda, S. K. *Science (Washington, D.C.)* **1984**, *223*, 69–71.

(5) Straub, K.; Kanne, D.; Hearst, J. E.; Rapoport, H. *J. Am. Chem. Soc.* **1981**, *103*, 2347–2355. Kanne, D.; Straub, K.; Hearst, J. E.; Rapoport, H. *J. Am. Chem. Soc.* **1982**, *104*, 6754–6764.

(6) Wei, T. T.; Byrne, K. M.; Warnick-Pickle, D.; Greenstein, M. *J. Antibiot.* **1982**, *35*, 545–548.

0022-3263/88/1953-3695$01.50/0